

SeasonDepth: Cross-Season Monocular Depth Prediction Dataset and Benchmark under Multiple Environments

Hanjiang Hu, *Student Member, IEEE*, Baoquan Yang, Zhijian Qiao, Ding Zhao, *Member, IEEE*, and Hesheng Wang, *Senior Member, IEEE*

Abstract—Different environments pose a great challenge to the outdoor robust visual perception for long-term autonomous driving and the generalization of learning-based algorithms on different environmental effects is still an open problem. Although monocular depth prediction has been well studied recently, there is few work focusing on the robust learning-based depth prediction across different environments, e.g. changing illumination and seasons, owing to the lack of such a multi-environment real-world dataset and benchmark. To this end, the first cross-season monocular depth prediction dataset and benchmark *SeasonDepth* is built based on *CMU Visual Localization* dataset. To benchmark the depth estimation performance under different environments, we investigate representative and recent state-of-the-art open-source supervised, self-supervised and domain adaptation depth prediction methods from *KITTI* benchmark using several newly-formulated metrics. Through extensive experimental evaluation on the proposed dataset, the influence of multiple environments on performance and robustness is analyzed qualitatively and quantitatively, showing that the long-term monocular depth prediction is still challenging even with fine-tuning. We further give promising avenues that self-supervised training and stereo geometry constraint help to enhance the robustness to changing environments. The dataset is available on <https://seasondepth.github.io>, and benchmark toolkit is available on <https://github.com/SeasonDepth/SeasonDepth>.

Index Terms—Monocular depth prediction, dataset and benchmark, long-term robust perception, autonomous driving



1 INTRODUCTION

VISUAL perception and localization for autonomous driving and mobile robotics has made significant progress due to the boost of deep convolutional neural networks [1, 2, 3, 4] in recent years. However, since the outdoor environmental conditions are changing because of different seasons, weather and daytime [5, 6, 7], the pixel-level appearance is drastically affected, which casts a big challenge for the robust long-term visual perception and localization. Monocular depth prediction plays a critical role in the long-term visual perception and localization [8, 9, 10, 11, 12] and is also significant to safe applications such as self-driving cars under different environmental conditions. Although some depth prediction datasets [13, 14, 15] include some different environments for diversity, it is still not clear what kind of algorithm is more robust to adverse conditions and how they influence depth prediction performance. Besides, the generalization of learning-based depth prediction methods on different weather and illumination effects is still an open problem. Therefore, building a new dataset and benchmark under multiple environments is needed to study this problem systematically. To the best of our knowledge, we are the first to study the generalization of learning-based depth prediction under changing environments, which is essential

and significant to both robust learning algorithms and practical applications like autonomous driving.

The outdoor high-quality dense depth maps are not easy to obtain using LiDAR or laser scanner projection [15, 16, 17], or stereo matching [13, 18, 19], let alone collections under multiple environments. We adopt Structure from Motion (SfM) and Multi-View Stereo (MVS) pipeline with RANSAC followed by careful manual post-processing to build a scaleless dense depth prediction dataset *SeasonDepth* with multi-environment traverses based on the urban part of CMU Visual Localization dataset [6, 20]. Some examples in the dataset are shown in Fig. 1.

For the benchmark on the proposed dataset, several statistical metrics are proposed for the experimental evaluation of the representative and state-of-the-art open-source methods from *KITTI* benchmark [16, 21]. The typical baselines we choose include supervised [1, 22, 23, 24], stereo training based self-supervised [25, 26, 27], monocular video based self-supervised [28, 29, 30, 31, 32] and domain adaptation [33, 34, 35] algorithms. Through thoroughly analyzing benchmark results, we find that no method can present satisfactory performance in terms of *Average*, *Variance* and *RelativeRange* metrics simultaneously even if some methods give impressive results on *KITTI* Eigen split [1] and are well fine-tuned on our training set. We further give hints of promising avenues to addressing this problem through self-supervised learning or stereo geometry constraint for model training. Furthermore, the performance under each environment is investigated both qualitatively and quantitatively for adverse environments.

For the open problem of generalizability of learning-

Corresponding author: Hesheng Wang

- H. Hu and D. Zhao are with the Department of Mechanical Engineering, Carnegie Mellon University, Pittsburgh, PA, 15213.
E-mail: hanjianghu@cmu.edu
- B. Yang, Z. Qiao and H. Wang are with the Department of Automation, Shanghai Jiao Tong University, Shanghai, China, 200240.
E-mail: wanghesheng@sjtu.edu.cn



Fig. 1. *SeasonDepth* samples with depth maps under *Cloudy + Foliage*, *Low Sun + Foliage*, *Cloudy + Mixed Foliage*, *Overcast + Mixed Foliage* and *Low Sun + Mixed Foliage*.

based depth prediction methods on different environmental conditions, our dataset is the first one that contains real-world RGB images with multiple environments under the same routes so that fair cross-environment evaluation can be conducted, giving hints to the future research on robust perception in changing environments. In summary, our contributions in this work are listed as follows.

- A new monocular depth prediction dataset *SeasonDepth* with the same multi-traverse routes under changing environments is introduced through SfM and MVS pipeline and is publicly available.
- We benchmark representative best open-sourced supervised, self-supervised, and domain adaptation depth prediction methods from *KITTI* leaderboard on *SeasonDepth* using several statistical metrics.
- From the extensive cross-environment evaluation, we point out that which kind of methods are robust to different environments and how changing environments affect the depth prediction to give future research directions.

The rest of the paper is structured as follows. Sec. 2 analyzes the related work about depth prediction datasets and algorithms. Sec. 3 presents the process of building *SeasonDepth*. Sec. 4 introduces the metrics and benchmark setup. The experimental evaluation and analysis are shown in Sec. 5. Finally, in Sec. 6 we give the conclusions.

2 RELATED WORK

2.1 Monocular Depth Prediction Datasets

Depth prediction plays an important role in the perception and localization of autonomous driving and other computer vision applications. Many indoor datasets are built through calibrated RGBD camera [36, 37, 38], expensive laser scanner [17, 40] and web stereo photos [14, 18, 19, 39]. However, outdoor depth maps as ground truth are more complex to get, *e.g.* projecting 3D point cloud data onto the image plane [15, 16, 17] for sparse map and using stereo matching to calculate inaccurate and limited-scope depth [13, 14, 18]. Another way to get the depth map is through SfM [15, 24, 41, 42] from monocular sequences. Although this method is time-consuming, it generates pretty accurate relatively-scaled dense depth maps, which is more general

for depth prediction under different scenarios. For the long-term robust perception under changing environments, though some real-world datasets [13, 14, 15] include some environmental changes, there are still no multi-environment traverses with the same routes, which is essential and necessary for fair evaluation of robustness across different environments. Since graphical rendering is becoming more and more realistic, some virtual synthetic datasets [43, 44, 45, 46] contain multi-environment traverses though the rendered RGB images are still different from real-world ones due to the domain gap and cannot be used to benchmark real-world cross-environment performance. The details of comparison between datasets are shown in Tab. 1 and Sec. 3.2.

2.2 Outdoor Monocular Depth Prediction Algorithms

The monocular depth prediction task aims to predict the dense depth map in an active way given one single RGB image. Early studies including MRF and other graph models [17, 47, 48] largely depend on man-made descriptors, constraining the performance of depth prediction. Afterwards, studies based on CNNs [1, 3, 49] have shown promising results for monocular depth estimation. Eigen *et al.* [1] first predict depth map using CNN model, while [3] introduces fully convolutional neural networks to regress the depth value. After that, supervised methods for monocular depth prediction have been well studied through normal estimation [23, 50], the supervision of depth map and stereo disparity ground truth [19, 22, 24, 51, 52]. However, since outdoor depth map ground truth is expensive and time-consuming to obtain, self-supervised depth estimation methods have appeared using stereo geometric left-right consistency [25, 26, 27, 53, 54, 55], egomotion-pose constraint through monocular video [28, 29, 30, 56, 57] and multi-task learning with optical flow, motion and semantics segmentation [31, 32, 58, 59] inside monocular video training pipeline as secondary supervisory signals. Besides, to avoid using expensive real-world depth map ground truth, other algorithms are trained on synthetic virtual datasets [43, 44, 45, 46] to leverage high-quality depth map ground truth with zero cost. Such methods [33, 34, 35, 60, 61] confront with the domain adaptation from synthetic to real-world domain only with supervision on virtual datasets for model training.

TABLE 1
Comparison between *SeasonDepth* and Other Datasets

Name	Scene	Real or Virtual	Depth Value	Sparse or Dense	Multiple Traverses	Different Environments
NYUV2 [36]	Indoor	Real	Absolute	Dense	×	×
DIML [37]	Indoor	Real	Absolute	Dense	×	×
iBims-1 [38]	Indoor	Real	Absolute	Dense	×	×
Make3D [17]	Outdoor & Indoor	Real	Absolute	Sparse	×	×
ReDWeb [18]	Outdoor & Indoor	Real	Relative	Dense	×	×
WSVD [39]	Outdoor & Indoor	Real	Relative	Dense	×	×
HR-WSI [19]	Outdoor & Indoor	Real	Absolute	Dense	×	×
DIODE [40]	Outdoor & Indoor	Real	Absolute	Dense	×	×
OASIS [41]	Outdoor & Indoor	Real	Relative	Dense	×	×
3D Movies [14]	Outdoor & Indoor	Real	Relative	Dense	×	✓
KITTI [16]	Outdoor	Real	Absolute	Sparse	×	×
Cityscapes [13]	Outdoor	Real	Absolute	Dense	×	✓
DIW [42]	Outdoor	Real	Relative	Sparse	×	×
MegaDepth [24]	Outdoor	Real	Relative	Dense	×	×
DDAD [29]	Outdoor	Real	Absolute	Dense	×	×
MPSD [15]	Outdoor	Real	Absolute	Dense	×	✓
V-KITTI [43]	Outdoor	Virtual	Absolute	Dense	✓	✓
SYNTHIA [44]	Outdoor	Virtual	Absolute	Dense	×	×
TartanAir [45]	Outdoor & Indoor	Virtual	Absolute	Dense	✓	✓
DeepGTAV [46]	Outdoor	Virtual	Absolute	Dense	✓	✓
SeasonDepth	Outdoor	Real	Relative	Dense	✓	✓

3 SEASONDEPTH DATASET

Our proposed dataset *SeasonDepth* is derived from CMU Visual Localization dataset [20] through SfM algorithm. The original CMU Visual Localization dataset covers over one year in Pittsburgh, USA, including 12 different environmental conditions. Images were collected from two identical cameras on the left and right of the vehicle along a route of 8.5 kilometers. And this dataset is also derived for long-term visual localization [6] by calculating the 6-DoF camera pose of images with more appropriate categories about the weather, vegetation and area. To be consistent with the content of driving scenes in other datasets like *KITTI*, we adopt images from Urban area categorized in [6] to build our dataset. More details about the dataset can be found in Supplementary Material Section 1.

3.1 Depth Dense Reconstruction and Post-processing

We reconstruct the dense model for each traversal under every environmental condition through SfM and MVS pipeline [62], which is commonly used for depth reconstruction [24, 29] and most suitable for multi-environment dense reconstruction for 3D mapping [6, 63] and show advantage on the aspects of high dense quality despite of huge computational efforts compared to active sensing from LiDAR. Specifically, similar to *MegaDepth* [24], COLMAP [62, 64] with SIFT descriptor [65] is used to obtain the depth maps through photometric and geometric consistency from sequential images. Furthermore, we adopt RANSAC algorithm in the SfM to remove the inaccurate values of dynamic objects in the images through effective modification in SIFT matching triangulation based on original COLMAP, where dynamic objects with additional motion besides relative camera motion do not obey the multi-view

geometry constraint and should be removed as noise via RANSAC in bundle adjustment optimization. Besides, from our justification experiments in Sec. 5.3, it is validated that using relative depth values and removing dynamic noise will not significantly influence the training and the performance of depth prediction models. Because the MVS algorithm generates the depth maps with error pixel values which are out of range or too close, like the cloud in the sky or noisy points on the very near road, we filter those outside the normal range of the depth map.

After the reconstruction, based on the observation of noise distribution in the HSV color space, *e.g.* blue pixels always appear in the sky and dark pixels always appear in the shade of low sun, which tend to be noise in most cases, we remove the noisy values in the HSV color space given some specific thresholds. Though outliers are set to be empty in RANSAC, instance segmentation is adopted through MaskRCNN [66] to fully remove the noise of dynamic objects. However, since it is difficult to generate accurate segmentation maps only for dynamic objects under drastically changing environments, we leverage human annotation as the last step to finally check the depth map. The data processing is shown in Fig. 2 with normalization after each step. Since we are rigorous and serious to the quality of valid depth pixels which are used for benchmark, we set most noise to be invalid (which causes some “holes” on the boundary from appearance) to avoid any possible pollution to the following benchmark, ensuring the reliable evaluation and benchmark results. More details can be found in Supplementary Material Section 1.1.

3.2 Comparison with Other Datasets

The current datasets are introduced in Sec. 2.1. The comparison between *SeasonDepth* and current datasets is shown

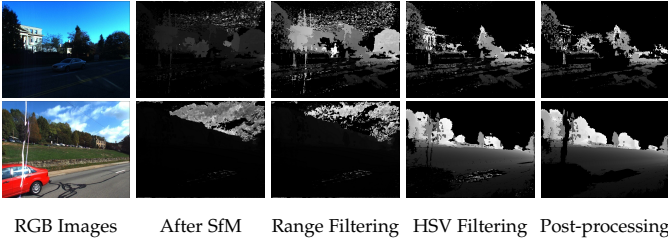


Fig. 2. The illustration of depth map processing.

in Tab. 1. The distinctive feature of the proposed dataset is that *SeasonDepth* contains comprehensive outdoor real-world multi-environment sequences with repeated scenes, just like virtual synthetic datasets [43, 45, 46] but they are rendered from computer graphics and suffer from the huge domain gap. Though real-world datasets [13, 14, 15] include different environments, they lack the same-route traverses under different conditions so they are not able to fairly evaluate the performance across changing environments. Similar to outdoor datasets [24, 41, 42], the depth maps of ours are scaleless with relative depth values, where the metrics should be designed for evaluation as the following section shows. The depth map ground truth from SfM is dense compared to LiDAR-based sparse depth maps. Besides, the comparison of depth value distribution is shown in Fig. 3. Note that the values of our dataset are scaleless and relative, so the x-axes of other datasets are also omitted for a fair comparison. We normalize the depth values for all the environments to mitigate the influence of the aggregation from relative depth distributions under different environments to get the final distribution map. The details of implementation can be found in Supplementary Material Section 1.2. From Fig. 3, it can be seen that our dataset also follows the long-tail distribution [67] which is the same as other datasets, with a difference of missing large-depth part due to range truncation during the building process in Sec. 3.1.

4 BENCHMARK SETUP

4.1 Evaluation Metrics

The challenge for the design of evaluation metrics lies in two folds. One is to cope with scaleless and partially-valid dense depth map ground truth, and the other is to fully measure the depth prediction average performance and the stability or robustness across different environments. Due to scaleless ground truth of relative depth value, some common metrics [21] cannot be used for evaluation directly. Since focal lengths of two cameras are close enough to generate similarly-distributed depth values, unlike [24, 28, 41], we align the distribution of depth prediction to depth ground truth via mean value and variance for a fair evaluation. The other key point for multi-environment evaluation lies in the reflection of robustness to changing environments for same-route sequences, which has not been studied in the previous work to the best of our knowledge. We formulate our metrics below.

First, for each pair of predicted and ground truth depth maps, the valid pixels $D_{valid_{predicted}}^{i,j}$ of the predicted depth map $D_{valid_{predicted}}$ are determined by non-empty valid pixels

$D_{valid_{GT}}^{i,j}$ of the depth map ground truth. And then the valid mean and variance of both $D_{valid_{GT}}$ and $D_{valid_{predicted}}$ are calculated as Avg_{GT}, Avg_{pred} and Var_{GT}, Var_{pred} . Then we adjust the predicted depth map D_{adj} to get the same distribution with $D_{valid_{GT}}$,

$$D_{adj} = (D_{pred} - Avg_{pred}) \times \sqrt{Var_{GT}/Var_{pred}} + Avg_{GT} \quad (1)$$

The examples of adjusted depth prediction are shown in Fig. 4. After this operation, we can eliminate scale difference for depth prediction across datasets, which makes this zero-shot evaluation on *SeasonDepth* reliable and applicable to all the models even though they predict absolute depth values, showing generalization ability on new datasets and robustness across different environments. Denote the adjusted valid depth prediction D_{adj} as D_P in the following formulation. To measure the depth prediction performance, we choose the most distinguishable metrics under multiple environments from commonly-used metrics in [21], *AbsRel* and $\delta < 1.25$ (a_1). For environment k , we have,

$$AbsRel^k = \frac{1}{n} \sum_{i,j} |D_P^k{}_{i,j} - D_{GT}^k{}_{i,j}| / D_{GT}^k{}_{i,j} \quad (2)$$

$$a_1^k = \frac{1}{n} \sum_{i,j} \mathbb{1}(\max\{\frac{D_P^k{}_{i,j}}{D_{GT}^k{}_{i,j}}, \frac{D_{GT}^k{}_{i,j}}{D_P^k{}_{i,j}}\} < 1.25) \quad (3)$$

For the evaluation under different environments, six secondary metrics are derived based on original metrics and statistics,

$$AbsRel^{avg} = \frac{1}{m} \sum_k AbsRel^k \quad (4)$$

$$AbsRel^{var} = \frac{1}{m} \sum_k \left| AbsRel^k - \frac{1}{m} \sum_k AbsRel^k \right|^2 \quad (5)$$

$$a_1^{avg} = \frac{1}{m} \sum_k a_1^k \quad (6)$$

$$a_1^{var} = \frac{1}{m} \sum_k \left| a_1^k - \frac{1}{m} \sum_k a_1^k \right|^2 \quad (7)$$

where *avg* terms $AbsRel^{avg}$, a_1^{avg} and *var* terms $AbsRel^{var}$, a_1^{var} come from *Mean* and *Variance* in statistics, indicating the average performance and the fluctuation around the mean value across multiple environments.

Considering the depth prediction applications, it should be more rigorous to prevent better results fluctuation than worse results under changing conditions. Therefore, we use the *Relative Range* terms $AbsRel^{relRng}$, a_1^{relRng} to calculate the relative difference of maximum and minimum for all the environments.

$$AbsRel^{relRng} = \frac{\max\{AbsRel^k\} - \min\{AbsRel^k\}}{\frac{1}{m} \sum_k AbsRel^k} \quad (8)$$

$$a_1^{relRng} = \frac{\max\{1 - a_1^k\} - \min\{1 - a_1^k\}}{\frac{1}{m} \sum_k (1 - a_1^k)} \quad (9)$$

Relative Range terms for $AbsRel$ and $1 - a_1$ are more strict than the *Variance* terms $AbsRel^{var}$, a_1^{var} and note that $1 - a_1$

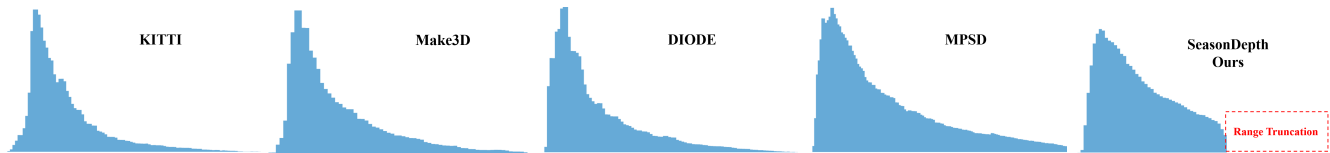


Fig. 3. Comparison of relative depth distributions of several datasets.



RGB and ground truth *PackNet* [29] *VNL* [23] *GASDA* [35]

Fig. 4. The examples of depth adjustment (from the first to second row) for prediction results.

instead of a_1 is used to calculate a_1^{relRng} to make relative range fluctuation more distinguishable for better methods.

4.2 Evaluated Algorithms

Following the category introduced in Sec. 2.2, we have chosen the representative baseline methods together with recent open-source state-of-the-art models on *KITTI* leaderboard [21] to evaluate the performance on the *SeasonDepth* dataset. The evaluated methods include supervised and self-supervised models trained on real-world images, and domain adaptation models trained on virtual synthetic images. For the **supervised models**, we choose *Eigen et al.* [1], *BTS* [22], *MegaDepth* [24] and *VNL* [23]. *Eigen et al.* propose the first method using CNNs to predict depth map with scale-invariant loss. *BTS* proposes novel multi-scale local planar guidance layers in decoders for full spatial resolution to get impressive ranked-4th performance. *MegaDepth* introduces an end-to-end hourglass network for depth prediction using semantic and geometric information as supervision. *VNL* proposes the virtual normal estimation which utilizes a stable geometric constraint for long-range relations in a global view to predict depth.

We further choose **self-supervised models** of stereo training, monocular video training and multi-task learning as secondary signals with video training. Previous work *Monodepth* [25] and two recent work *adareg* [26], *monoResMatch* [27] are evaluated to present the performance of models trained with stereo geometric constraint. For joint pose regression and depth prediction using video sequences, we test the first method *SfMLearner* [28] and two recent methods *Monodepth2* [30], *PackNet* [29], where *Monodepth2* model also involves stereo geometric information in model training. Besides, we evaluate *CC* [31] with optical flow estimation and motion segmentation, and *SGDepth* [32] with supervised semantic segmentation inside the monocular video based self-supervised framework. For **domain adaptation models** trained on the virtual dataset with multiple environments, we evaluate several recent competitive algorithms Atapour

et al. [33], *T2Net* [34] and *GASDA* [35]. Atapour *et al.* [33] use CycleGAN [68] to train depth predictor with translated synthetic images using virtual ground truth from DeepGTAV [46]. *T2Net* is a fully supervised method both on *KITTI* and *V-KITTI* dataset and it enables synthetic-to-real translation and depth prediction simultaneously. But *GASDA* is self-supervised for real-world images by incorporating geometry-aware loss through wrapping stereo images together with image translation from synthetic to the real-world domain. More details about the benchmark models including fine-tuning details can be found in Supplementary Material Section 2.1.

5 EXPERIMENTAL EVALUATION RESULTS

5.1 Evaluation Comparison from Overall Metrics

In this section, we analyze and discuss what kinds of algorithms are more robust to changing environments by giving several main findings and their impacts on performance. The quantitative results of open-source best depth prediction baselines can be found in Tab. 2. To alleviate the impact of dataset bias between *KITTI* and *SeasonDepth*, we adopt the held-out training set to fine-tune one supervised [22] and one self-supervised model [28], which initially perform poor zero-shot results. Since our dataset does not contain stereo images, segmentation ground truth, and *KITTI*-like scenarios, just like in *V-KITTI*, the stereo training based, semantic segmentation involved multi-task training and domain adaptation models are omitted for the sake of fairness.

Analysis of fine-tuning To make sure the findings and claims are predominantly owing to the different conditions instead of domain shift, the fine-tuning analysis is first presented before other critical findings for this problem. The best fine-tuned results of *Average* are chosen in Tab. 2 together with the corresponding *Variance* and *RelativeRange* results. Based on Fig. 5 with shadows of cross-slice standard deviation after zooming 0.5, 0.2, and 0.5 times, it can be seen that after the fine-tuning, overall performance is improved while some *Variance* and *RelativeRange* results still perform badly, especially for *SfMLearner* [28]. More analysis about model training can be found in Sec. 5.3. Consequently, fine-tuning gives limited help to the robustness to changing environments though overall performance is better because of reducing the domain gap, indicating that solely increasing the variability of training data cannot address the challenge of environmental changes. To make the evaluation and comparison fair, we draw our conclusion regardless they are fine-tuned or not. *Variance* and *RelativeRange* metrics are convincing to reflect robustness across different environments.

Supervised vs self-supervised methods Basically, self-supervised methods show more robustness to different

TABLE 2
SeasonDepth Benchmark Results (↓: Lower Better, ↑: Higher Better, **Best**, **Second Best**)

Method	KITTI Eigen Split		<i>SeasonDepth</i> : Average		Variance(10^{-2})		Relative Range		
	<i>AbsRel</i> ↓	a_1 ↑	<i>AbsRel</i> ↓	a_1 ↑	<i>AbsRel</i> ↓	a_1 ↓	<i>AbsRel</i> ↓	$1 - a_1$ ↓	
Supervised	Eigen <i>et al.</i> [1]	0.203	0.702	1.093	0.340	0.346	0.0170	0.206	0.0746
	BTS [22]	0.060	0.955	0.676	0.209	0.545	0.0650	0.405	0.129
	BTS (fine-tuned)	—	—	<u>0.339</u>	0.479	0.0425	0.0389	0.203	0.117
	MegaDepth [24]	0.220	0.632	0.515	0.417	0.0874	0.0285	0.200	0.107
	VNL [23]	<u>0.072</u>	<u>0.938</u>	0.306	0.527	0.126	0.166	0.400	0.290
Self-supervised Stereo Training	Monodepth [25]	0.148	0.803	0.436	0.455	<u>0.0475</u>	<u>0.0213</u>	0.198	0.104
	adareg [26]	0.126	0.840	0.507	0.405	0.0630	0.0474	<u>0.178</u>	0.0137
	monoResMatch [27]	0.096	0.890	0.487	0.389	0.286	0.0871	0.414	0.160
Self-supervised Monocular Video Training	SfMLearner [28]	0.181	0.733	0.360	0.495	0.0801	0.0628	0.269	0.182
	SfMLearner (fine-tuned)	—	—	0.413	0.440	0.0502	0.0290	0.177	0.100
	PackNet [29]	0.116	0.865	0.722	0.421	0.187	0.0705	0.186	0.155
	Monodepth2 [30]	0.106	0.874	0.420	0.429	0.0848	0.0907	0.229	0.188
	CC [31]	0.140	0.826	0.648	0.479	0.223	0.0881	0.280	0.241
SGDepth [32]	0.113	0.879	0.648	0.480	0.0987	0.0498	0.197	0.169	
Syn-to-real Domain Adaptation	Atapour <i>et al.</i> [33]	0.110	0.923	0.687	0.300	0.224	0.0220	0.231	<u>0.0622</u>
	T2Net [34]	0.169	0.769	0.827	0.391	0.399	0.0799	0.286	0.146
	GASDA [35]	0.143	0.836	0.438	0.411	0.121	0.0665	0.271	0.145

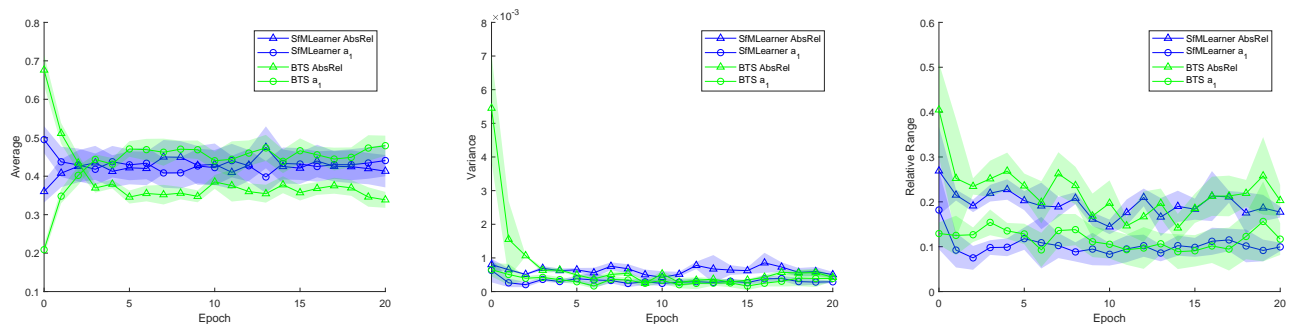


Fig. 5. Performance evolution after fine-tuning on *SeasonDepth* training set.

environments than supervised ones. Supervised methods suffer from large values of *Variance* and *RelativeRange* across multiple environments compared to self-supervised methods, showing that supervised methods are more sensitive to changing environments and even fine-tuning cannot critically improve the cross-environment performance. Besides, although the first proposed several depth prediction methods [1, 25, 28, 33] perform worse than recent methods on overall *Average*, they show impressive stability to different environments through low *Variance* and *RelativeRange*.

Effectiveness of stereo training Inside the self-supervised methods, stereo training based methods [25, 26, 27] are more robust to different environments than monocular video training based [28, 29] and multi-task learning [31, 32] methods from *Variance* and *RelativeRange*. Coming broadly to monocular video training and syn-to-real models, training with stereo geometry constraint [30, 35] is clearly beneficial to improve the robustness to the changing environments compared to those without it, as shown quantitatively with light blue shades in Tab. 2 and qualitatively with underlines in Fig. 8. Interestingly, the methods with good *Variance* performance are not consistent with those with good *Average* performance, which indicates that algorithms tend to work well in specific environments

instead of being effective and robust to all conditions, validating the significance of the cross-environment study with *SeasonDepth* dataset.

Qualitative analysis Qualitative results for different types of baselines are shown in Fig. 8. It can be seen that supervised methods *BTS* [22] and *VNL* [23] suffer from overfitting through the predicted pattern where the top and bottom areas are dark while the central areas are light, even for buildings. Stereo training involved methods with underlines [30, 35] perform continuous depth results for the same entity under all environments, *e.g.* the depth prediction of buildings compared to other self-supervised monocular (S-Sup-M) video based methods [29, 32] and syn-to-real (Syn-to-Real) domain adaptation method [34], validating the improvement of robustness using stereo geometry constraint like quantitative results in Tab. 2. See Supplementary Material Section 2.2 for more qualitative results and analysis.

5.2 Performance under Different Environment Conditions

In this section, we further study how different environments influence the depth prediction results. Different from how different methods perform under multiple environments, this section investigate which environment is more difficult

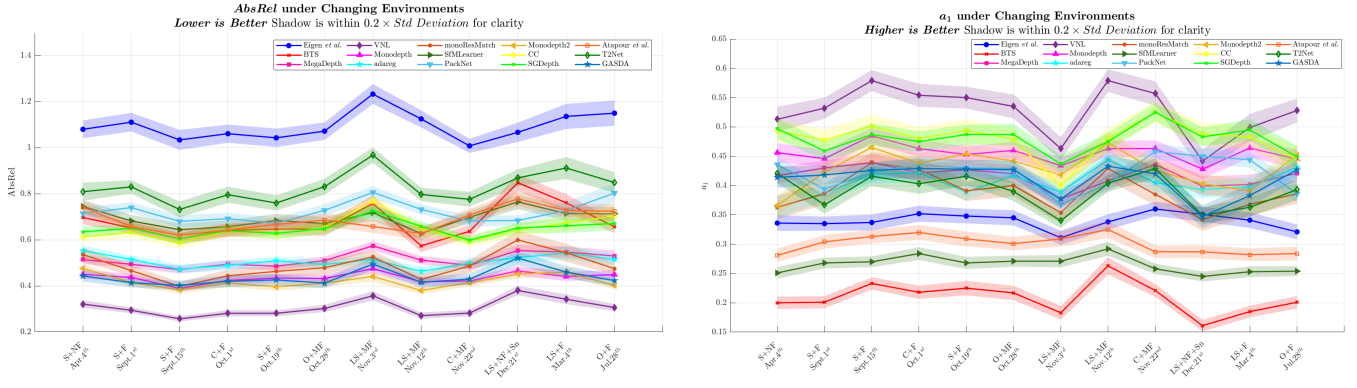


Fig. 6. Results on *SeasonDepth* dataset under 12 different environments with dates. The shadows indicate error bars around mean values with $0.2 \times \text{Standard Deviation}$ for more clarity.

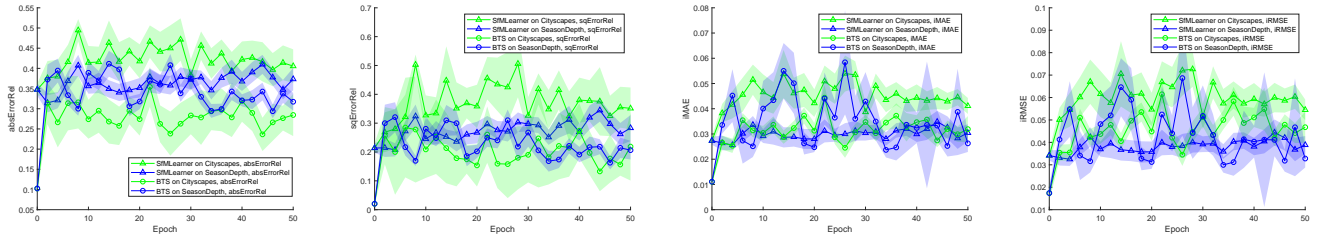


Fig. 7. Cross-dataset quantitative performance evolution on KITTI validation set [21] with models fine-tuned on *SeasonDepth* and *Cityscapes* [13].

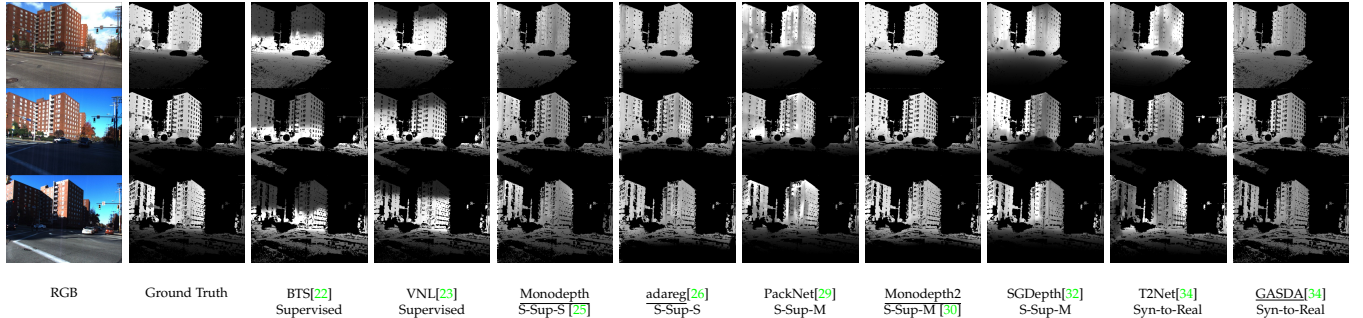


Fig. 8. Comparison among supervised, self-supervised stereo based (S-Sup-S), self-supervised monocular video based (S-Sup-M) and domain adaptation (Syn-to-Real) methods. Underlines are denoted for training with stereo geometry constraint.

to the current depth prediction models. The line chart with shadow error bar in Fig. 6 shows performance in changing environments intuitively. The abbreviations of environments are *S* for *Sunny*, *C* for *Cloudy*, *O* for *Overcast*, *LS* for *Low Sun*, *Sn* for *Snow*, *F* for *Foliage*, *NF* for *No Foliage*, and *MF* for *Mixed Foliage*.

Influence of different environments From Fig. 6, we can see that although different methods perform differently on *AbsRel* and α_1 , the influence of some environments is similar for all the methods. Most methods perform well under *S+F*, *Sept. 15th* and *LS+MF*, *Nov. 12th* while dusk scenes in *LS+MF*, *Nov. 3rd* and snowy scenes in *LS+NF+Sn*, *Dec. 21st* pose great challenge for most algorithms, which points out directions for future research and safe applications. Besides, the error bar in Fig. 6 shows adverse environments always result in large deviations for all algorithms, indicating adverse environments influence the results of all the methods.

Promising methods for adverse environments Under

these adverse environmental conditions, the promising algorithms can also be found. For the dusk or snowy scenes, although training with virtual synthetic images with multiple environments through domain adaptation [33, 34, 35] helps little for the overall metrics, some of domain adaptation methods [33, 34] present impressive robustness under adverse scenes due to the various appearances of synthetic images. For the snowy scenes, self-supervised stereo-based [25, 26, 30] and monocular video training models [29, 31, 32] are less influenced compared to supervised methods.

Qualitative analysis Qualitative experimental results in Fig. 10 show how extreme illumination or vegetation changes affect the depth prediction. We visualize the adjusted results of three overall good methods with robustness to changing environments according to Sec. 5.1 and Tab. 2. From the top two rows, it can be seen that illumination change of low sun makes the depth prediction of tree trunks less clear under the same vegetation condition as green and red blocks

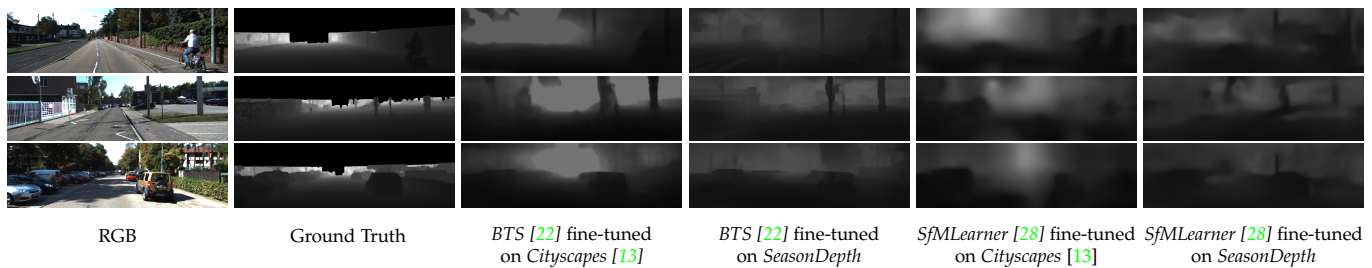


Fig. 9. Qualitative comparison results on KITTI validation set [21] with depth prediction models fine-tuned on *SeasonDepth* and *Cityscapes* [13]

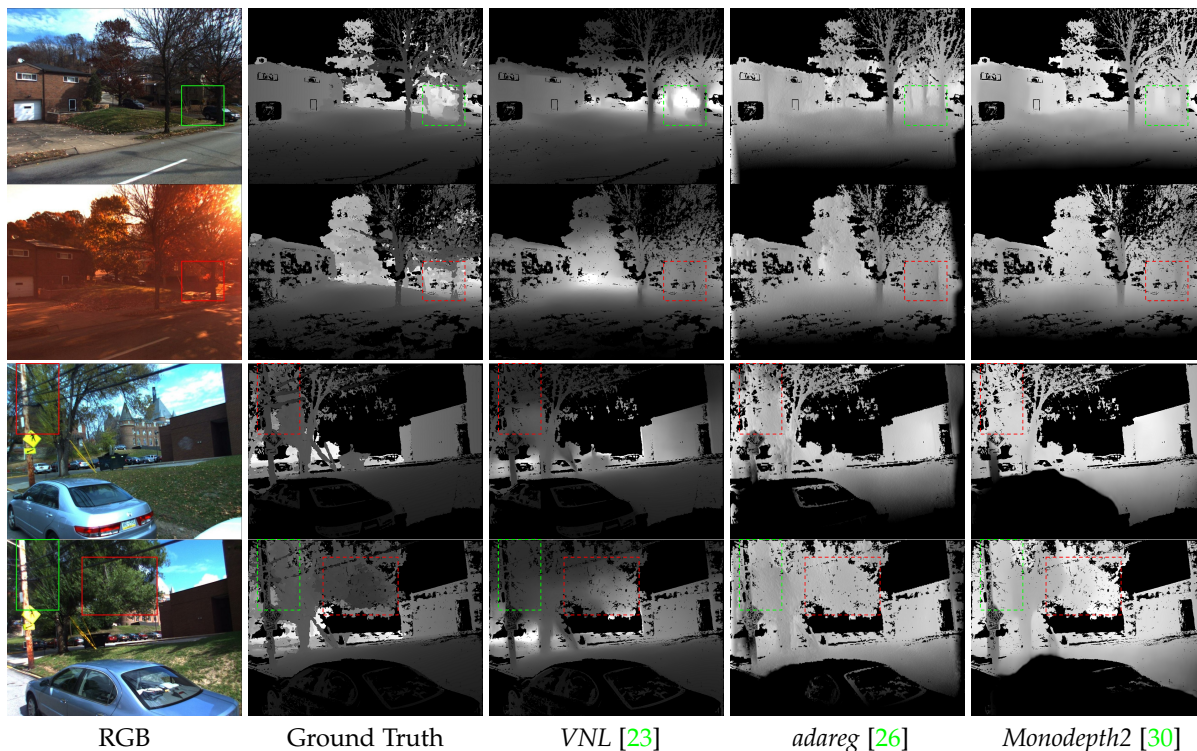


Fig. 10. Qualitative comparison results with illumination or vegetation changes. The conditions from top to down are *C+MF, Nov. 22nd*, *LS+MF, Nov. 3rd*, *C+MF, Nov. 22nd* and *C+F, Oct. 1st*. Green blocks indicate good performance while red blocks are for bad results.

show. Also, no foliage tends to make telephone pole and tree trunk less distinguishable by comparing red and green blocks from the last two rows, while the depth prediction of heavy vegetation is difficult as red blocks show on the fourth row given the same illumination and weather condition. More qualitative and detailed results with mean values and standard deviations can be found in Supplementary Material Section 2.2.

5.3 Justification of *SeasonDepth* Used for Model Training

Since the lack of dynamic objects in our dataset, we further conduct more experiment to justify that the depth accuracy and the ground truth are good enough for the dataset usage of autonomous driving for model training. Specifically, inspired by cross-dataset transfer degradation evaluation in [14], we compare our dataset with the stereo depth dataset *Cityscapes* [13] in terms of the degraded performance on KITTI dataset after cross-dataset fine-tuning. Using the

same pre-trained models on KITTI as introduced in the last section, we fine-tune BTS [22] and SfMLearner [28] models on *SeasonDepth* and *Cityscapes* dataset with the same amount of images, and evaluate the per-epoch depth prediction on KITTI validation set via the metrics of *AbsRel*, *SqRel*, *iMAE* and *iRMSE* from [21]. The shadows show the range of metrics after centering and zooming 0.02, 0.01, 0.035 and 0.04 times for clarity. More details can be found in Supplementary Material Section 2.3.

From the quantitative results in Fig. 7, we can see that although the performance will be degraded compared to the KITTI pre-trained models due to domain shift when fine-tuning, the performance fine-tuned on *SeasonDepth* is better than models fine-tuned on *Cityscapes*, especially for *SfMLearner* method and *iMAE* and *iRMSE* metrics. Besides, the fluctuation of models fine-tuned on *SeasonDepth* is much less than those fine-tuned on *Cityscapes* in terms of *AbsRel* and *SqRel* metrics. Based on the qualitative performance in Fig. 9, we can find that models fine-tuned on *SeasonDepth* perform better than those fine-tuned on *Cityscapes* on the

unseen KITTI dataset. Consequently, although the depth maps of *SeasonDepth* are reconstructed from structure from motion and do not contain dynamic objects, the ground truth accuracy is eligible to be used for model training compared to the stereo depth dataset *Cityscapes*, justifying our ground truth accuracy is adequate though it is not perfect.

5.4 Further Discussion

In this section, we will discuss how to improve the robustness across multiple environments methodologically to boost more research on long-term robust visual perception. Research about long-term performance under changing environments stems from visual place recognition and localization. Most of deep learning based methods leverage environmentally-insensitive perceptual auxiliary information like semantic [69, 70], geometric [71, 72], context-aware [73, 74] information, or learn the domain-invariant representation [75, 76] or image translation [10, 77] in multi-domain setting.

Our work targets the robustness of these auxiliary perceptual tasks, evaluating the best monocular depth prediction methods under different environments. The findings from our benchmark are intuitively environmentally-insensitive, *e.g.*, stereo geometric constraint, multi-task learning with semantic segmentation. Following the methodology and taxonomy of long-term visual place recognition methods, many potential models can be developed using our dataset and benchmark, like domain-invariant feature-based methods, attention mechanism involved methods *etc.*

6 CONCLUSION

In this paper, a new dataset *SeasonDepth* is built for monocular depth prediction under different environments, and supervised, self-supervised, and domain adaptation open-source algorithms from *KITTI* leaderboard are evaluated. From the experimental results, we find that there is still a long way to go to achieve robustness for long-term depth prediction and several promising avenues are given. Self-supervised methods present better robustness than supervised methods to changing environments, and stereo geometry involved training also helps under cross-environment cases. Through studying how adverse environments influence, our findings via this dataset and benchmark will impact the research on long-term robust perception and related applications.

APPENDIX A

BUILDING SEASONDEPTH DATASET

In this section, we present more details about the process of building *SeasonDepth* dataset and statistical analysis of depth maps in each environment.

A.1 Details in Building Dataset

We adopt the categorized slices of the Urban part according to [6] as original images after rectification through camera intrinsic file. Specifically, we use `slice2`, `slice3`, `slice7`, `slice8` as the split test slices for evaluation and benchmark, and the other slices `slice4`, `slice5`, `slice6` are intended to treat as training sets. Note that

since not all images from the original dataset are appropriate for depth prediction due to huge noise, *e.g.*, a moving truck covering almost all the pixels, we remove such images in the final version. The released dataset split can be found on <https://seasondepth.github.io/>. The numbers of images under all the environments for all slices in training set and test set are shown in Tab. 3. The abbreviations of environments are S for Sunny, C for Cloudy, O for Overcast, LS for Low Sun, Sn for Snow, F for Foliage, NF for No Foliage, and MF for Mixed Foliage. It could be seen that the total number of test set is larger than that of training set with more different slices, which helps to make the benchmark results more accurate and reliable. Also, the training set can be used to fine-tune pre-trained models, which do not need too many images. Images from left and right cameras are merged together in the same slice for calculation.

We adopt COLMAP’s MVS pipeline [62, 64] to find the 3D structure and depth map. We follow the instruction on <https://colmap.github.io/> with sequential SIFT matching with RANSAC, sparse reconstruction, and dense reconstruction. Some important detailed hyperparameters can be found in Tab. 4, while others are with the default configuration. To make full use of the image sequences, we adjust the sequential matching overlap to be 15 instead of the whole sequence, improving the local optimization with less noise. During each iteration of RANSAC algorithm in triangulation, the minimum inlier ratio for SIFT matching is set to be 0.65 for the consideration that most pixels of a single image are static in most cases. The maximum SIFT matching distance is 0.55 to adapt the distance of dynamic objects and improve efficiency. The image samples after SfM can be found in Fig. 11-(b)

The valid pixels of the original depth map are between the lower threshold and upper threshold to filter most noise pixels. For one thing, since the fields, forests, and cloud in the far distance away from the camera matter little to the depth prediction applications for autonomous driving, we truncate the depth values over 92% (80% in some cases) of the whole image to focus more on the near roads, vehicles, buildings, vegetation, *etc.* For another, due to the camera placement on both sides of the car, the very near descriptors of the road cannot be correctly matched during SfM and reconstructed for dense depth map, which should be removed by filtering the pixel values less than 5% of the whole depth map. Besides, in the special cases that all the near-road noises appear on the bottom of the images, we directly filter the pixels with depth values greater than a threshold in that rectangular bottom area of the images. The samples after depth range truncation can be seen in Fig. 11-(c).

Although depth range truncation removes some pixels with too large depth values, there are still misreconstructed pixels of sky, cloud or shadow with normal depth values. We use *PowerToys* from <https://github.com/microsoft/PowerToys> to pick up typical HSV values for further refinement and denoising. As Tab. 5 shows, the minimal and maximal HSV values are given for some typical noises, including sky, cloud, reflections and shadows. For the clear or cloudy sky, Value tends to be high around 200 and Hue is usually blue or white. However, for those areas in the shadow of low sun, Saturation and Value are extremely low to be about 10% so that the depth map pixels are too hard to be correctly

TABLE 3
Numbers of Images under All the Environments for All Slices

Environments	Training Set				Test Set				
	slice4	slice5	slice6	All Slices	slice2	slice3	slice7	slice8	All Slices
S+NF Apr. 4th	221	129	543	893	382	450	190	449	1471
S+F Sept. 1st	116	230	190	536	385	464	249	490	1588
S+F Sept. 15th	202	213	526	941	335	329	462	457	1583
C+F Oct. 1st	406	205	626	1237	347	438	350	244	1379
S+F Oct. 19th	288	192	558	1038	301	439	412	230	1382
O+MF Oct. 28th	394	194	536	1124	333	418	362	442	1555
LS+MF Nov. 3rd	445	198	399	1042	335	447	203	416	1401
LS+MF Nov. 12th	0	221	552	762	352	500	357	501	1710
C+MF Nov. 22nd	323	163	578	1064	298	436	380	423	1537
LS+NF+Sn Dec. 21st	241	14	592	847	284	512	56	147	999
LS+F Mar. 4th	175	19	498	692	354	222	0	512	1088
O+F Jul. 28th	458	212	560	1230	256	425	384	467	1532
All Environments	3269	1980	6158	11407	3962	5080	3405	4778	17225

reconstructed, which need to be filtered. The samples after HSV refinement are shown in Fig. 11-(d).

Though RANSAC algorithm inside the SfM and MVS pipeline largely removes pixels of the dynamic objects to ensure the accuracy of overall depth values, the dynamic pixels cannot be fully eliminated and the contours of objects are not clear as well. Therefore, we employ MaskRCNN [66] with pre-trained models from Detectron2 on <https://github.com/facebookresearch/detectron2>. We adopt the pre-trained model with configuration file of *COCO-InstanceSegmentation/mask_rcnn_R50_FPN_3x.yaml* and modify the `MODEL.ROI_HEADS.SCORE_THRESH_TEST` to be 0.5 to find the instance segmentation with the class of car, person and bus. To process the image directly, we modify the visualization part in the official colab notebook, omitting boxes, keypoints and labels and letting $\alpha = 1$ in `draw_polygon` function to set the pixels of the target objects to be black. But semantic or instance segmentation cannot distinguish dynamic objects that need to be removed, we use human annotation to check whether segmented vehicles or pedestrians are moving or not, relabeling the missing dynamic objects and correcting the mislabeled objects. The depth map samples after all the post-processing can be found in Fig. 11-(e). Note that since there are often more misreconstructed depth pixels around thin objects like branches and poles, we manually filter some of them in the processing

for accuracy and reliable evaluation.

A.2 Statistics and Analysis of Depth Map for Each Environment

Here we give the statistical analysis of the proposed *SeasonDepth* dataset for each environment. Since all the depth values are scale-free and not absolute for distance, it is not applicable to directly find the pixel value distribution for the dataset as [29, 40] do. However, the depth values of sequential frames in similar urban scenes under the same environment are similarly distributed, *i.e.* the depth of images along the similar streets and blocks are consistent. Then the key point is to align the distribution of each environment to the mean of all environments, obtaining the normalized whole distribution map and dismissing the scale discrepancy.

Therefore, we first find the original depth value distribution $p_{D_i}(x)$ for all the slices under each environment i . Then lower quartile Q_1 (25%), median Q_2 (50%) and upper quartile Q_3 (75%) are calculated for the original distribution of every environment and the mean value of quartiles can be found as reference quartiles $Q_{1_{ref}}, Q_{2_{ref}}, Q_{3_{ref}}$ for all n environments,

$$Q_{1_{ref}} = \frac{1}{n} \sum_{i=1}^n Q_{1_i}, Q_{2_{ref}} = \frac{1}{n} \sum_{i=1}^n Q_{2_i}, Q_{3_{ref}} = \frac{1}{n} \sum_{i=1}^n Q_{3_i}$$



Fig. 11. The processing samples given RGB image followed by normalized depth maps for clear visualization of (a) dense reconstruction, (b) range filtering, (c) HSV-based refinement and (d) manual post-processing.

TABLE 4
Some Important Hyperparameters for COLMAP

Process	Hyperparameter	Value
Sequential SIFT Matching	min_inlier_ratio	0.65
	max_distance	0.55
	min_num_inliers	50
	overlap_num	15
RANSAC	dyn_num_trials_multiplier	3.0
	confidence	0.99
	min_inlier_ratio	0.1
Sparse Reconstucion	abs_pose_min_inlier_ratio	0.25
	filter_max_reproj_error	4.0
	filter_min_tri_angle	1.5
Dense Reconstucion	geom_consistency_max_cost	3.0
	geom_consistency_regularizer	0.3

TABLE 5
Some Typical Noises and HSV Thresholds

Noise Source and Type	minimal threshold (H, S, V)	maximal threshold (H, S, V)
Blue Sky	(172, 5%, 40%)	(240, 90%, 100%)
White Cloud and Bright Reflections from Windows	(0, 0%, 100%)	(360, 100%, 100%)
Dark and Black Shadows	(0, 0%, 0%)	(0, 0%, 0)%
Dusk Cloud and Refections from Roads and Cars	(0, 0%, 70%)	(90, 20%, 100%)
Dusk Sky	(140, 11%, 40%)	(160, 50%, 100%)

To find the scale normalization ratio r_i , we use arithmetic mean to measure the ratio of reference quartiles $Q_{1_{ref}}, Q_{2_{ref}}, Q_{3_{ref}}$ and other quartiles $Q_{1_i}, Q_{2_i}, Q_{3_i}$,

$$r_i = \frac{1}{3} \left(\frac{Q_{1_{ref}}}{Q_{1_i}} + \frac{Q_{2_{ref}}}{Q_{2_i}} + \frac{Q_{3_{ref}}}{Q_{3_i}} \right) \quad (10)$$

Then the distribution $p_{D_i}(x)$ can be normalized to mean reference environment to obtain $p_{D_{norm_i}}(x)$,

$$p_{D_{norm_i}}(x) = r_i p_{D_i}(x) \quad (11)$$

After that, the normalized distribution of all the environments can be added directly to get the whole distribution. The distribution map of each environment can be found in Fig. 12. It can be seen that all the pixels follow a similar long-tail distribution, and the average y-axis numbers of per-image pixels overcome the bias caused by unbalanced image quantities across different environments. The normalization makes each distribution aligned on the x-axis, which can be directly added to obtain the total distribution map, as Fig.3 in the main body paper shows.

APPENDIX B SEASONDEPTH BENCHMARK

B.1 Details about Evaluated Models

For the fairness to evaluate the performance of off-the-shelf depth prediction algorithms under changing environments, we investigate a large amount of depth prediction methods and choose to benchmark the representative and recent

state-of-the-art supervised, self-supervised, and domain adaptation models from well-known *KITTI* leaderboard [21], which are with open-source codes and pre-trained models for a fair comparison. Here give important details for all the evaluated baselines. Our experiments are conducted on two NVIDIA 2080Ti cards with 64G RAM on Ubuntu 18.04 system. The evaluation metrics are modified based on development kit [21] on http://www.cvlibs.net/dataset/s/kitti/eval_depth.php?benchmark=depth_prediction. Also, our fine-tuned models on the SeasonDepth training set can be found on our website <https://seasondepth.github.io/>.

For the supervised methods, we evaluate four representative methods, Eigen *et al.* [1], *BTS* [22], *MegaDepth* [24] *VNL* [23]. Eigen *et al.* propose the first CNNs-based depth prediction method and introduce the famous Eigen split of *KITTI* dataset for depth prediction benchmark. We hence evaluate this representative method through <https://github.com/DhruvJawalkar/Depth-Map-Prediction-from-a-Single-Image-using-a-Multi-Scale-Deep-Network> with the improved image gradient component in the newer loss to see the performance across multiple environments. Recent supervised work *BTS* ranks 4th on *KITTI* benchmark and we test it on <https://github.com/cogaplex-bts/bts> using the pre-trained model *DenseNet161* on Eigen split. We further fine-tune this pre-trained model of *BTS* on our training set for 20 epochs with a batch size of 16. The best performance of *Average* metric is obtained from epoch 20. Due to the scaleless and partially validated ground truth, we only calculate the non-zero pixels and

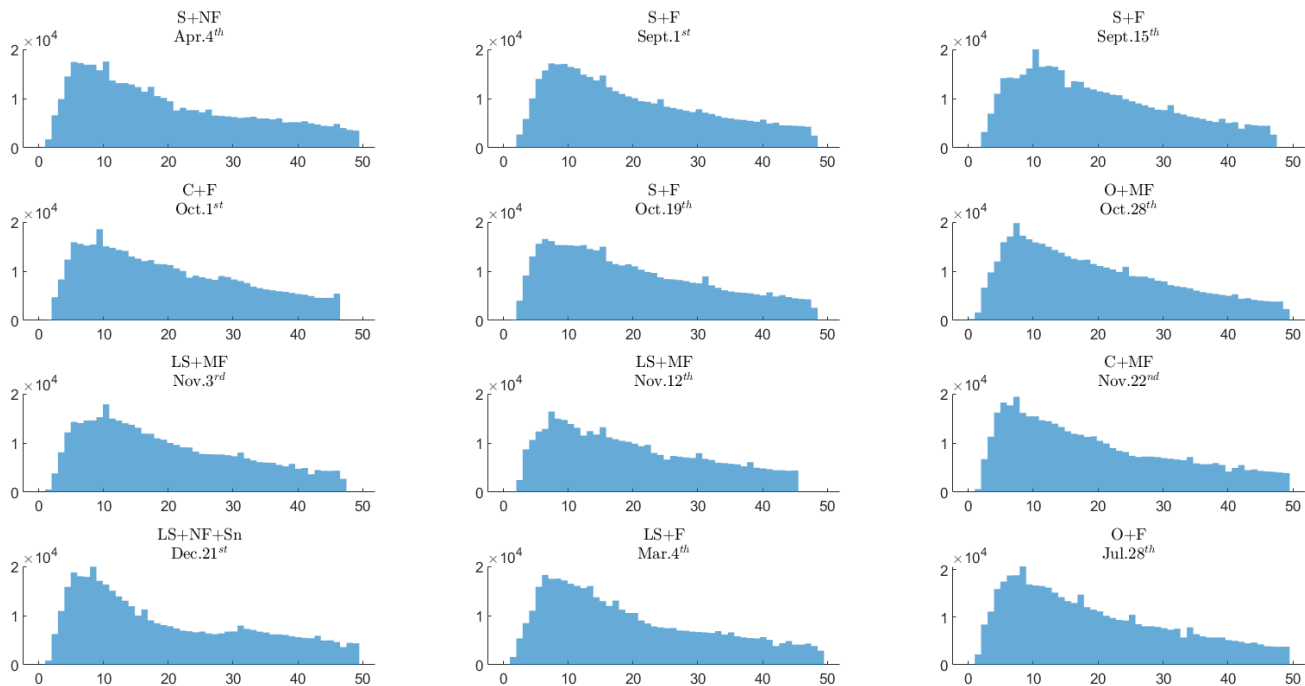


Fig. 12. The normalized depth map distribution under all environments. The values of y-axes are number of pixels with the value of abscissa on each image on average.

conduct alignment using the mean value for loss when fine-tuning. Note that focal value does not influence the experimental results due to the relative scale of the depth metrics. We test *MegaDepth* method according to <https://www.cs.cornell.edu/projects/megadepth/> with the *MegaDepth* pre-trained models as described in the paper and all the hyperparameters are set as default. *VNL* are evaluated using https://github.com/YvanYin/VNL_Monocular_Depth_Prediction with the pre-trained model of ResNext101_32x4d backbone and trained on *KITTI* dataset.

For self-supervised methods, we further categorize them and choose baselines respectively, *i.e.* *Monodepth* [25], *adareg* [26] and *monoResMatch* [27] for stereo geometry based methods, *SfmLearner* [28], *Monodepth2* [30] and *PackNet* [29] for monocular video SfM based methods, and *CC* [31] and *SGDepth* [32] for multi-task learning with monocular SfM unsupervised pipeline. For stereo geometry based unsupervised methods, *Monodepth* method is evaluated using <https://github.com/OniroAI/MonoDepth-PyTorch>, which is able to reproduce similar results to those in the paper on Eigen split. We test the model of *adareg* from <https://github.com/alexklwong/adareg-monodispnet> pre-trained with Eigen split. *monoResMatch* is tested through <https://github.com/fabiotosi92/monoResMatch-Tensorflow> with *KITTI* pretrained model with default hyperparameters. For sequence SfM based unsupervised methods, we adopt <https://github.com/ClementPinard/SfmLearner-Pytorch> to benchmark *SfmLearner* for better performance than original repo with slight modification. We further fine-tune the pre-trained models of *dispnet_model_best* and *exp_pose_model_best* on our training set using default configuration file with sequence length of 5 for 20 epochs

to get the best performance on *Average* metric at epoch 20. We use the model of ResNet18 pre-trained on *ImageNet* and fine-tuned on *KITTI* with the resolution of 640×192 to test *PackNet* on <https://github.com/TRI-ML/packnet-sfm>. Similarly, in order to incorporate stereo geometric constraint into the monocular SfM framework, we use the model of *mono+stereo* pre-trained on *ImageNet* and *KITTI* with the resolution of 640×192 to evaluate the performance of *Monodepth2* on <https://github.com/nianticlabs/monodepth2>. For the multi-task SfM unsupervised learning methods, *CC* is evaluated with *DispNet*, *PoseNet*, *MaskNet* and *FlowNet* pre-trained model on *KITTI* through <https://github.com/anuragranj/cc>. We also test another recent work *SGDepth* on <https://github.com/ifnspaml/SGDepth> with the full model of semantic segmentation and depth prediction with the resolution of 640×192 .

Since synthetic datasets like *V-KITTI* include multiple environments in spite of existing domain gap, we additionally evaluate the performance of three domain adaptation methods from *KITTI* benchmark, *Atapour et al.* [33], *T2Net* [34] and *GASDA* [35]. We follow the instruction on <https://github.com/atapour/monocularDepth-Inference> to evaluate the method proposed by *Atapour et al.* with the model pre-trained on *KITTI* and *DeepGTAV* [46]. *T2Net* is tested on <https://github.com/lyndonzheng/Synthetic2Realistic> with the weakly-supervised pre-trained model for outdoor scenes of *KITTI* and *V-KITTI*. We then evaluate the performance of *GASDA* on <https://github.com/sshan-zhao/GASDA> with the model pre-trained on *V-KITTI* and *KITTI* using self-supervised stereo geometric information.

TABLE 6
AbsRel Results (Lower Better) under Each Environment: Mean(Standard Deviation)

Method	S+NF Apr. 4th	S+F Sept. 1st	S+F Sept. 15th	C+F Oct. 1st	S+F Oct. 19th	O+MF Oct. 28th	LS+MF Nov. 3rd	LS+MF Nov. 12th	C+MF Nov. 22nd	LS+NF+S Dec. 21st	LS+F Mar. 4th	O+F Jul. 28th
Eigen <i>et al.</i> [1]	1.080(0.39)	1.111(0.40)	1.034(0.43)	1.061(0.40)	1.043(0.40)	1.072(0.38)	1.233(0.43)	1.125(0.37)	1.008(0.32)	1.067(0.42)	1.136(0.54)	1.150(0.55)
BTS [22]	0.697(0.29)	0.652(0.24)	0.605(0.24)	0.641(0.29)	0.647(0.27)	0.646(0.28)	0.758(0.35)	0.574(0.27)	0.637(0.27)	0.848(0.36)	0.761(0.38)	0.657(0.28)
MegaDepth [24]	0.514(0.20)	0.494(0.16)	0.471(0.17)	0.494(0.18)	0.486(0.18)	0.510(0.18)	0.574(0.21)	0.512(0.18)	0.489(0.19)	0.553(0.26)	0.547(0.25)	0.530(0.24)
VNL [23]	0.321(0.16)	0.294(0.13)	0.257(0.11)	0.281(0.14)	0.281(0.13)	0.302(0.16)	0.357(0.20)	0.271(0.14)	0.282(0.14)	0.380(0.21)	0.342(0.21)	0.306(0.15)
Monodepth [25]	0.450(0.19)	0.437(0.16)	0.389(0.14)	0.424(0.18)	0.434(0.18)	0.432(0.16)	0.475(0.20)	0.418(0.17)	0.421(0.16)	0.465(0.21)	0.441(0.20)	0.449(0.20)
adareg [26]	0.553(0.22)	0.515(0.16)	0.473(0.18)	0.489(0.20)	0.509(0.19)	0.493(0.19)	0.515(0.17)	0.463(0.18)	0.498(0.20)	0.523(0.20)	0.543(0.29)	0.515(0.25)
monoResMatch [27]	0.536(0.31)	0.466(0.24)	0.398(0.19)	0.444(0.27)	0.463(0.25)	0.479(0.31)	0.526(0.28)	0.428(0.25)	0.486(0.28)	0.600(0.40)	0.544(0.39)	0.475(0.26)
SfMLearner [28]	0.745(0.29)	0.682(0.26)	0.644(0.27)	0.657(0.28)	0.684(0.29)	0.671(0.28)	0.718(0.35)	0.627(0.27)	0.698(0.27)	0.765(0.32)	0.714(0.29)	0.713(0.31)
PackNet [29]	0.715(0.27)	0.740(0.23)	0.680(0.26)	0.692(0.26)	0.672(0.24)	0.728(0.27)	0.806(0.27)	0.732(0.22)	0.682(0.25)	0.684(0.22)	0.727(0.36)	0.803(0.43)
Monodepth2 [30]	0.476(0.18)	0.414(0.15)	0.383(0.17)	0.412(0.17)	0.396(0.17)	0.412(0.17)	0.441(0.23)	0.380(0.16)	0.414(0.16)	0.452(0.20)	0.459(0.20)	0.402(0.16)
CC [31]	0.613(0.23)	0.633(0.23)	0.587(0.25)	0.640(0.24)	0.627(0.27)	0.652(0.24)	0.768(0.25)	0.649(0.23)	0.593(0.24)	0.649(0.28)	0.673(0.34)	0.703(0.39)
SGDepth [32]	0.635(0.24)	0.650(0.21)	0.605(0.23)	0.640(0.23)	0.628(0.23)	0.649(0.24)	0.726(0.26)	0.659(0.20)	0.599(0.19)	0.651(0.23)	0.661(0.31)	0.671(0.29)
Atapour <i>et al.</i> [33]	0.741(0.27)	0.658(0.22)	0.619(0.24)	0.643(0.27)	0.667(0.27)	0.686(0.29)	0.658(0.28)	0.627(0.29)	0.708(0.27)	0.778(0.32)	0.728(0.29)	0.724(0.30)
T2Net [34]	0.809(0.39)	0.830(0.29)	0.732(0.34)	0.796(0.35)	0.760(0.33)	0.831(0.35)	0.968(0.33)	0.797(0.29)	0.776(0.33)	0.869(0.37)	0.912(0.48)	0.849(0.45)
GASDA [35]	0.443(0.24)	0.414(0.20)	0.402(0.21)	0.420(0.26)	0.426(0.24)	0.412(0.22)	0.495(0.26)	0.416(0.24)	0.429(0.24)	0.521(0.29)	0.460(0.26)	0.423(0.26)

TABLE 7
 α_1 Results (Higher Better) under Each Environment: Mean(Standard Deviation)

Method	S+NF Apr. 4th	S+F Sept. 1st	S+F Sept. 15th	C+F Oct. 1st	S+F Oct. 19th	O+MF Oct. 28th	LS+MF Nov. 3rd	LS+MF Nov. 12th	C+MF Nov. 22nd	LS+NF+S Dec. 21st	LS+F Mar. 4th	O+F Jul. 28th
Eigen <i>et al.</i> [1]	0.336(0.14)	0.335(0.12)	0.337(0.14)	0.352(0.14)	0.348(0.13)	0.345(0.13)	0.311(0.12)	0.338(0.13)	0.360(0.12)	0.351(0.13)	0.341(0.13)	0.321(0.13)
BTS [22]	0.200(0.11)	0.201(0.10)	0.233(0.10)	0.218(0.11)	0.225(0.12)	0.217(0.12)	0.183(0.12)	0.263(0.15)	0.221(0.11)	0.161(0.10)	0.185(0.10)	0.201(0.11)
MegaDepth [24]	0.417(0.14)	0.430(0.13)	0.439(0.15)	0.422(0.16)	0.427(0.13)	0.420(0.15)	0.377(0.13)	0.408(0.15)	0.436(0.15)	0.399(0.17)	0.402(0.17)	0.421(0.15)
VNL [23]	0.513(0.21)	0.532(0.18)	0.579(0.18)	0.554(0.20)	0.550(0.19)	0.535(0.20)	0.463(0.20)	0.579(0.19)	0.557(0.21)	0.442(0.19)	0.499(0.23)	0.528(0.21)
Monodepth [25]	0.456(0.17)	0.446(0.15)	0.485(0.13)	0.463(0.15)	0.453(0.14)	0.460(0.15)	0.434(0.14)	0.463(0.14)	0.463(0.14)	0.428(0.17)	0.464(0.16)	0.445(0.15)
adareg [26]	0.363(0.18)	0.387(0.14)	0.419(0.15)	0.422(0.17)	0.389(0.14)	0.417(0.15)	0.389(0.15)	0.444(0.16)	0.405(0.17)	0.393(0.15)	0.398(0.16)	0.431(0.18)
monoResMatch [27]	0.363(0.21)	0.386(0.18)	0.439(0.18)	0.428(0.20)	0.391(0.17)	0.400(0.19)	0.354(0.18)	0.439(0.20)	0.385(0.19)	0.342(0.19)	0.368(0.20)	0.386(0.17)
SfMLearner [28]	0.251(0.10)	0.268(0.09)	0.270(0.09)	0.284(0.11)	0.268(0.11)	0.271(0.10)	0.271(0.11)	0.292(0.12)	0.258(0.09)	0.245(0.09)	0.253(0.09)	0.254(0.09)
PackNet [29]	0.436(0.13)	0.394(0.13)	0.422(0.15)	0.435(0.15)	0.430(0.14)	0.429(0.14)	0.368(0.13)	0.403(0.12)	0.458(0.13)	0.450(0.13)	0.444(0.14)	0.386(0.17)
Monodepth2 [30]	0.366(0.17)	0.423(0.16)	0.465(0.19)	0.438(0.17)	0.454(0.18)	0.442(0.16)	0.418(0.19)	0.473(0.18)	0.426(0.17)	0.403(0.17)	0.391(0.18)	0.452(0.16)
CC [31]	0.493(0.19)	0.478(0.18)	0.501(0.21)	0.480(0.20)	0.494(0.19)	0.479(0.19)	0.400(0.15)	0.480(0.18)	0.525(0.18)	0.488(0.19)	0.483(0.20)	0.445(0.21)
SGDepth [32]	0.497(0.17)	0.459(0.16)	0.487(0.19)	0.475(0.18)	0.487(0.17)	0.487(0.18)	0.437(0.14)	0.475(0.15)	0.525(0.15)	0.483(0.16)	0.495(0.18)	0.449(0.19)
Atapour <i>et al.</i> [33]	0.281(0.12)	0.304(0.12)	0.313(0.12)	0.320(0.13)	0.309(0.13)	0.301(0.11)	0.309(0.13)	0.325(0.15)	0.287(0.11)	0.287(0.11)	0.282(0.11)	0.284(0.12)
T2Net [34]	0.421(0.17)	0.367(0.15)	0.416(0.17)	0.403(0.17)	0.416(0.16)	0.390(0.16)	0.304(0.13)	0.404(0.15)	0.429(0.17)	0.349(0.14)	0.363(0.16)	0.393(0.17)
GASDA [35]	0.414(0.18)	0.418(0.16)	0.426(0.14)	0.429(0.17)	0.428(0.16)	0.427(0.15)	0.377(0.16)	0.433(0.18)	0.420(0.17)	0.347(0.19)	0.383(0.19)	0.427(0.16)

B.2 Detailed Evaluation Results across Environments

In this section, the detailed results with mean values and standard deviations are shown in Tab. 6 and Tab. 7, it can be seen that models with larger mean values tend to have more significant deviation for each environment. However, though some large standard deviations in Tab. 6 and Tab. 7 weaken the credibility and reliability for the performance of methods, the quality of depth map ground truths is assured. So we attribute it to the poor generalization ability of those algorithms since not all the methods present such poor results with too large variances, which cannot be correctly analyzed.

Moreover, all the evaluated baselines are visualized after adjustment under typical challenging environments, including dark illumination, snowy scene, and complex vegetation. See Fig. 13 for more details. From the results of supervised methods, it can be seen that the patterns of predicted depth maps are similar, especially for *BTS* [22] and *VNL* [23], where the top and bottom areas are dark while the middle areas are bright due to overfitting, see buildings as examples. But *VNL* [23] shows advantage on depth details (e.g. telephone poles and vegetation) in the middle areas which accounts for the best average performance.

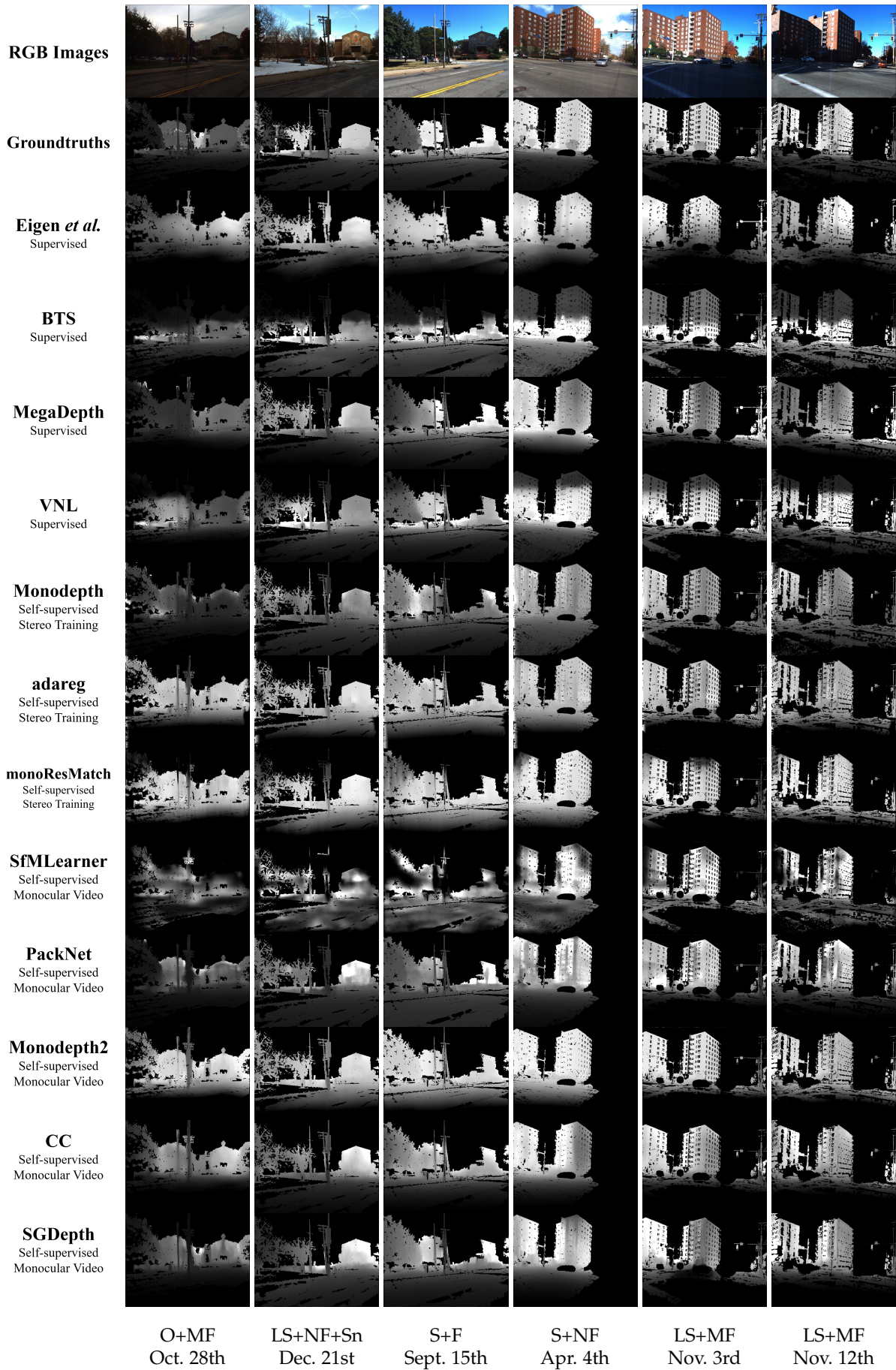
Stereo training involved self-supervised methods (including *Monodepth2* [30] and *GASDA* [35]) perform best continuous depth results for the same entity under all environments, e.g. depth values of buildings. Monocular video-based self-supervised methods do better in distinguishing relative depth from far and near areas, e.g. depth values for objects along different directions of roads, especially for multi-task learning ones *CC* [31] and *SGDepth* [32]. Besides,

domain adaptation methods still suffer from domain gaps, which shows that synthetic multi-environment images help little to improve performance under real-world changing environments.

B.3 Details about Cross-dataset Justification on KITTI

In this section, we present more details about the cross-dataset experiment to justify our depth quality for model training. As it is introduced in Sec. B.1, we choose the KITTI pre-trained models for *BTS* and *SfMLearner* methods, and fine-tune them on our training set and *Cityscapes* [13] for 50 epochs, respectively. Finally, we evaluate the cross-dataset transfer performance on KITTI validation set [21] using development kit from http://www.cvlibs.net/dataset/s/kitti/eval_depth.php?benchmark=depth_prediction. We choose 11407 images from `train_extra` in *Cityscapes* [13] to fine-tune the models, which is exactly the same amount of images in our training set to make the comparison fair.

To fine-tune the self-supervised model of *SfMLearner*, we set `batch_size` to be 4, `epoch_size` to be 1000 and `sequence_length` to be 1000. Along with the instructions to train with own data <https://github.com/ClementPinaud/SfmLearner-Pytorch/issues/108>, we crop a quarter of the bottom in the image and resize it to be 416×128 to remove the car logo in *Cityscapes* dataset. We change the intrinsic parameters accordingly to make them consistent with cropped images. For a fair comparison, we also conduct such cropping for the images from *SeasonDepth* dataset. When testing the KITTI validation set, we resize the images to be 416×128 before feeding them into the networks.



To be continued

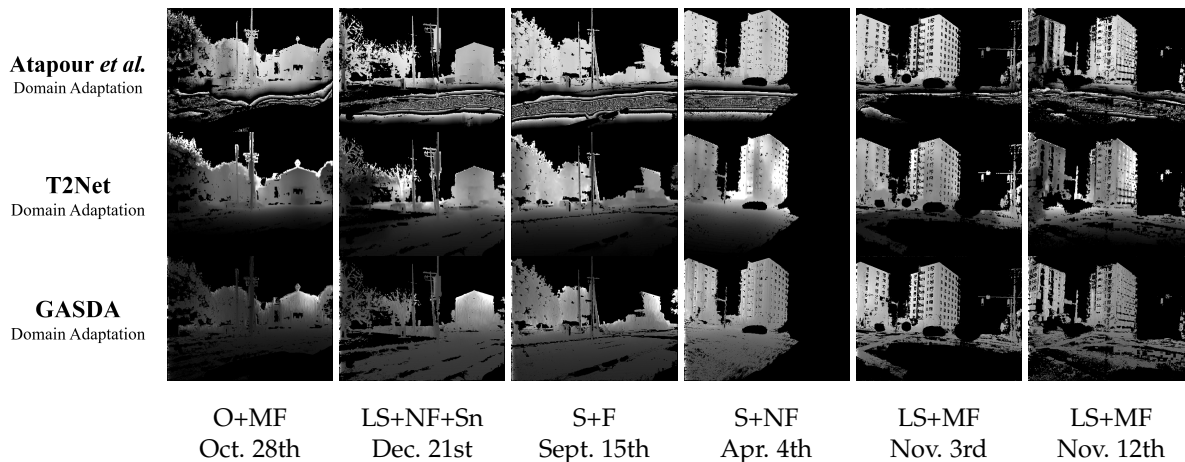


Fig. 13. Qualitative results for all the baselines with multiple illumination, vegetation and weather conditions.

When fine-tuning supervised *BTS* model, we set `batch_size` to be 16, `input_size` to be 256×192 for *SeasonDepth* images and 256×128 for *Cityscapes* images. For depth ground truth, we directly adopt the depth maps in *Cityscapes* as supervision signals while for *SeasonDepth* dataset, we only consider the non-zero pixels and conduct alignment using mean value to the ground truth to construct loss when fine-tuning. The experimental results show that such alignment to construct supervised loss is effective using our dataset for supervised model training.

APPENDIX C LIMITATION AND DISCUSSION

In this section, we discuss the limitation of our work. As mentioned before, our *SeasonDepth* dataset is built based on CMU Visual Localization dataset, which was initially collected for visual localization and contained multiple scenes but without challenging night scenes. Although it is different from the dataset for autonomous driving like *KITTI*, which causes concern about the evaluation due to the domain gap. However, based on the experimental evidence, it is acceptable that fine-tuned models only provide limited help in terms of *Variance* and *RelativeRange*. Although dynamic objects are not included in the dataset to ensure accuracy and reliability, it does not affect the evaluation for real driving applications because it cannot be distinguished whether the objects are dynamic or static given a single monocular image when testing. And the cross-dataset justification experiment also shows that missing dynamic objects do not influence the model training too much. Consequently, the evaluation of the depth prediction of static objects can reveal the performance of dynamic objects, although they are not involved in the ground truth.

Besides, though normalizing the scale of evaluation metrics through alignment of mean and variance can also be done through quantile alignment shown in Sec A.2, it is more sensitive to noise to adopt quantile-based alignment of every single image for evaluation. Although we try our best to survey and test the open-source representative models as much as possible, it is impossible to involve all the monocular depth prediction methods in our benchmark. So we will

release the test set and benchmark toolkit to make up for it. Another limitation is that it is not straightforward to train models on the dataset because of the ground truths of scaleless relative values, but it can be trained after the mean value alignment to the ground truth just as the fine-tuned *BTS* does. It can also reflect how environmental changes affect depth prediction models and give hints of what kind of method is more promising to this problem.

REFERENCES

- [1] David Eigen, Christian Puhrsch, and Rob Fergus. Depth map prediction from a single image using a multi-scale deep network. In *Advances in neural information processing systems*, pages 2366–2374, 2014.
- [2] Fayao Liu, Chunhua Shen, Guosheng Lin, and Ian Reid. Learning depth from single monocular images using deep convolutional neural fields. *IEEE transactions on pattern analysis and machine intelligence*, 38(10):2024–2039, 2015.
- [3] Iro Laina, Christian Rupprecht, Vasileios Belagiannis, Federico Tombari, and Nassir Navab. Deeper depth prediction with fully convolutional residual networks. In *2016 Fourth international conference on 3D vision (3DV)*, pages 239–248. IEEE, 2016.
- [4] Dan Xu, Elisa Ricci, Wanli Ouyang, Xiaogang Wang, and Nicu Sebe. Multi-scale continuous crfs as sequential deep networks for monocular depth estimation. In *Proceedings of the IEEE Conference on Computer Vision and Pattern Recognition*, pages 5354–5362, 2017.
- [5] Will Maddern, Geoffrey Pascoe, Chris Linegar, and Paul Newman. 1 year, 1000 km: The oxford robotcar dataset. *The International Journal of Robotics Research*, 36(1):3–15, 2017.
- [6] Torsten Sattler, Will Maddern, Carl Toft, Akihiko Torii, Lars Hammarstrand, Erik Stenborg, Daniel Safari, Masatoshi Okutomi, Marc Pollefeys, Josef Sivic, et al. Benchmarking 6dof outdoor visual localization in changing conditions. In *Proceedings of the IEEE Conference on Computer Vision and Pattern Recognition*, pages 8601–8610, 2018. <https://www.visuallocalization.net/>.

- [7] Zhe Liu, Shunbo Zhou, Chuanzhe Suo, Peng Yin, Wen Chen, Hesheng Wang, Haoang Li, and Yun-Hui Liu. Lpd-net: 3d point cloud learning for large-scale place recognition and environment analysis. In *Proceedings of the IEEE International Conference on Computer Vision*, pages 2831–2840, 2019.
- [8] Qunjie Zhou, Torsten Sattler, and Laura Leal-Taixe. Patch2pix: Epipolar-guided pixel-level correspondences. 2021.
- [9] Mans Larsson, Erik Stenborg, Carl Toft, Lars Hammarstrand, Torsten Sattler, and Fredrik Kahl. Fine-grained segmentation networks: Self-supervised segmentation for improved long-term visual localization. In *Proceedings of the IEEE International Conference on Computer Vision*, pages 31–41, 2019.
- [10] Tomas Jenicek and Ondrej Chum. No fear of the dark: Image retrieval under varying illumination conditions. In *Proceedings of the IEEE International Conference on Computer Vision*, pages 9696–9704, 2019.
- [11] Hanjiang Hu, Zhijian Qiao, Ming Cheng, Zhe Liu, and Hesheng Wang. Dsgil: Domain adaptation for semantic and geometric-aware image-based localization. *IEEE Transactions on Image Processing*, 30:1342–1353, 2020.
- [12] Nathan Piasco, Desire Sidibe, Valerie Gouet-Brunet, and Cedric Demonceaux. Improving image description with auxiliary modality for visual localization in challenging conditions. *International Journal of Computer Vision*, 129(1):185–202, 2021.
- [13] Marius Cordts, Mohamed Omran, Sebastian Ramos, Timo Rehfeld, Markus Enzweiler, Rodrigo Benenson, Uwe Franke, Stefan Roth, and Bernt Schiele. The cityscapes dataset for semantic urban scene understanding. In *Proceedings of the IEEE conference on computer vision and pattern recognition*, pages 3213–3223, 2016.
- [14] René Ranftl, Katrin Lasinger, David Hafner, Konrad Schindler, and Vladlen Koltun. Towards robust monocular depth estimation: Mixing datasets for zero-shot cross-dataset transfer. *IEEE Transactions on Pattern Analysis and Machine Intelligence*, 2020.
- [15] Manuel López Antequera, Pau Gargallo, Markus Hofinger, Samuel Rota Bulò, Yubin Kuang, and Peter Kontschieder. Mapillary planet-scale depth dataset. In *European Conference on Computer Vision*, pages 589–604. Springer, 2020.
- [16] Andreas Geiger, Philip Lenz, and Raquel Urtasun. Are we ready for autonomous driving? the kitti vision benchmark suite. In *2012 IEEE Conference on Computer Vision and Pattern Recognition*, pages 3354–3361. IEEE, 2012.
- [17] Ashutosh Saxena, Min Sun, and Andrew Y Ng. Make3d: Learning 3d scene structure from a single still image. *IEEE transactions on pattern analysis and machine intelligence*, 31(5):824–840, 2008.
- [18] Ke Xian, Chunhua Shen, Zhiguo Cao, Hao Lu, Yang Xiao, Ruibo Li, and Zhenbo Luo. Monocular relative depth perception with web stereo data supervision. In *The IEEE Conference on Computer Vision and Pattern Recognition (CVPR)*, June 2018.
- [19] Ke Xian, Jianming Zhang, Oliver Wang, Long Mai, Zhe Lin, and Zhiguo Cao. Structure-guided ranking loss for single image depth prediction. In *Proceedings of the IEEE/CVF Conference on Computer Vision and Pattern Recognition*, pages 611–620, 2020.
- [20] Hernán Badino, Daniel Huber, and Takeo Kanade. Visual topometric localization. In *2011 IEEE Intelligent Vehicles Symposium (IV)*, pages 794–799. IEEE, 2011.
- [21] Jonas Uhrig, Nick Schneider, Lukas Schneider, Uwe Franke, Thomas Brox, and Andreas Geiger. Sparsity invariant cnns. In *International Conference on 3D Vision (3DV)*, 2017.
- [22] Jin Han Lee, Myung-Kyu Han, Dong Wook Ko, and Il Hong Suh. From big to small: Multi-scale local planar guidance for monocular depth estimation. *arXiv preprint arXiv:1907.10326*, 2019.
- [23] Wei Yin, Yifan Liu, Chunhua Shen, and Youliang Yan. Enforcing geometric constraints of virtual normal for depth prediction. In *Proceedings of the IEEE International Conference on Computer Vision*, pages 5684–5693, 2019.
- [24] Zhengqi Li and Noah Snavely. Megadepth: Learning single-view depth prediction from internet photos. In *Proceedings of the IEEE Conference on Computer Vision and Pattern Recognition*, pages 2041–2050, 2018.
- [25] Clément Godard, Oisín Mac Aodha, and Gabriel J Brostow. Unsupervised monocular depth estimation with left-right consistency. In *Proceedings of the IEEE Conference on Computer Vision and Pattern Recognition*, pages 270–279, 2017.
- [26] Alex Wong and Stefano Soatto. Bilateral cyclic constraint and adaptive regularization for unsupervised monocular depth prediction. In *Proceedings of the IEEE Conference on Computer Vision and Pattern Recognition*, pages 5644–5653, 2019.
- [27] Fabio Tosi, Filippo Aleotti, Matteo Poggi, and Stefano Mattoccia. Learning monocular depth estimation infusing traditional stereo knowledge. In *Proceedings of the IEEE Conference on Computer Vision and Pattern Recognition*, pages 9799–9809, 2019.
- [28] Tinghui Zhou, Matthew Brown, Noah Snavely, and David G Lowe. Unsupervised learning of depth and ego-motion from video. In *Proceedings of the IEEE Conference on Computer Vision and Pattern Recognition*, pages 1851–1858, 2017.
- [29] Vitor Guizilini, Rares Ambrus, Sudeep Pillai, Allan Raventos, and Adrien Gaidon. 3d packing for self-supervised monocular depth estimation. In *Proceedings of the IEEE/CVF Conference on Computer Vision and Pattern Recognition*, pages 2485–2494, 2020.
- [30] Clément Godard, Oisín Mac Aodha, Michael Firman, and Gabriel J Brostow. Digging into self-supervised monocular depth estimation. In *Proceedings of the IEEE International Conference on Computer Vision*, pages 3828–3838, 2019.
- [31] Anurag Ranjan, Varun Jampani, Lukas Balles, Kihwan Kim, Deqing Sun, Jonas Wulff, and Michael J Black. Competitive collaboration: Joint unsupervised learning of depth, camera motion, optical flow and motion segmentation. In *Proceedings of the IEEE/CVF Conference on Computer Vision and Pattern Recognition*, pages 12240–12249, 2019.
- [32] Marvin Klingner, Jan-Aike Termöhlen, Jonas Mikolajczyk, and Tim Fingscheidt. Self-supervised monocular depth estimation: Solving the dynamic object problem

- by semantic guidance. In *European Conference on Computer Vision*, pages 582–600. Springer, 2020.
- [33] Amir Atapour-Abarghouei and Toby P Breckon. Real-time monocular depth estimation using synthetic data with domain adaptation via image style transfer. In *Proceedings of the IEEE Conference on Computer Vision and Pattern Recognition*, pages 2800–2810, 2018.
- [34] Chuanxia Zheng, Tat-Jen Cham, and Jianfei Cai. T2net: Synthetic-to-realistic translation for solving single-image depth estimation tasks. In *Proceedings of the European Conference on Computer Vision (ECCV)*, pages 767–783, 2018.
- [35] Shanshan Zhao, Huan Fu, Mingming Gong, and Dacheng Tao. Geometry-aware symmetric domain adaptation for monocular depth estimation. In *Proceedings of the IEEE Conference on Computer Vision and Pattern Recognition*, pages 9788–9798, 2019.
- [36] Nathan Silberman, Derek Hoiem, Pushmeet Kohli, and Rob Fergus. Indoor segmentation and support inference from rgb-d images. In *European conference on computer vision*, pages 746–760. Springer, 2012.
- [37] Youngjung Kim, Hyungjoo Jung, Dongbo Min, and Kwanghoon Sohn. Deep monocular depth estimation via integration of global and local predictions. *IEEE transactions on Image Processing*, 27(8):4131–4144, 2018.
- [38] Tobias Koch, Lukas Liebel, Friedrich Fraundorfer, and Marco Körner. Evaluation of cnn-based single-image depth estimation methods. In Laura Leal-Taixé and Stefan Roth, editors, *European Conference on Computer Vision Workshop (ECCV-WS)*, pages 331–348. Springer International Publishing, 2018.
- [39] Chaoyang Wang, Simon Lucey, Federico Perazzi, and Oliver Wang. Web stereo video supervision for depth prediction from dynamic scenes. In *2019 International Conference on 3D Vision (3DV)*, pages 348–357. IEEE, 2019.
- [40] Igor Vasiljevic, Nick Kolkin, Shanyi Zhang, Ruotian Luo, Haochen Wang, Falcon Z Dai, Andrea F Daniele, Mohammadreza Mostajabi, Steven Basart, Matthew R Walter, et al. Diode: A dense indoor and outdoor depth dataset. *arXiv preprint arXiv:1908.00463*, 2019.
- [41] Weifeng Chen, Shengyi Qian, David Fan, Noriyuki Kojima, Max Hamilton, and Jia Deng. Oasis: A large-scale dataset for single image 3d in the wild. In *Proceedings of the IEEE/CVF Conference on Computer Vision and Pattern Recognition*, pages 679–688, 2020.
- [42] Weifeng Chen, Zhao Fu, Dawei Yang, and Jia Deng. Single-image depth perception in the wild. In *Advances in neural information processing systems*, pages 730–738, 2016.
- [43] Adrien Gaidon, Qiao Wang, Yohann Cabon, and Eleonora Vig. Virtual worlds as proxy for multi-object tracking analysis. In *Proceedings of the IEEE conference on computer vision and pattern recognition*, pages 4340–4349, 2016.
- [44] German Ros, Laura Sellart, Joanna Materzynska, David Vazquez, and Antonio M Lopez. The synthia dataset: A large collection of synthetic images for semantic segmentation of urban scenes. In *Proceedings of the IEEE conference on computer vision and pattern recognition*, pages 3234–3243, 2016.
- [45] Wenshan Wang, Delong Zhu, Xiangwei Wang, Yaoyu Hu, Yuheng Qiu, Chen Wang, Yafei Hu, Ashish Kapoor, and Sebastian Scherer. Tartanair: A dataset to push the limits of visual slam. In *2020 IEEE/RSJ International Conference on Intelligent Robots and Systems (IROS)*, pages 4909–4916, 2020.
- [46] Aitor Ruano Miralles. An open-source development environment for self-driving vehicles. <http://openaccess.uoc.edu/webapps/o2/bitstream/10609/63765/6/aruanomTFM0617memory.pdf>, 2017.
- [47] Ashutosh Saxena, Sung H Chung, and Andrew Y Ng. Learning depth from single monocular images. In *Advances in neural information processing systems*, pages 1161–1168, 2006.
- [48] Beyang Liu, Stephen Gould, and Daphne Koller. Single image depth estimation from predicted semantic labels. In *2010 IEEE Computer Society Conference on Computer Vision and Pattern Recognition*, pages 1253–1260. IEEE, 2010.
- [49] David Eigen and Rob Fergus. Predicting depth, surface normals and semantic labels with a common multi-scale convolutional architecture. In *Proceedings of the IEEE international conference on computer vision*, pages 2650–2658, 2015.
- [50] Uday Kusupati, Shuo Cheng, Rui Chen, and Hao Su. Normal assisted stereo depth estimation. In *Proceedings of the IEEE/CVF Conference on Computer Vision and Pattern Recognition (CVPR)*, June 2020.
- [51] Huan Fu, Mingming Gong, Chaohui Wang, Kayhan Batmanghelich, and Dacheng Tao. Deep ordinal regression network for monocular depth estimation. In *Proceedings of the IEEE Conference on Computer Vision and Pattern Recognition*, pages 2002–2011, 2018.
- [52] Siyuan Qiao, Yukun Zhu, Hartwig Adam, Alan Yuille, and Liang-Chieh Chen. Vip-deeplab: Learning visual perception with depth-aware video panoptic segmentation. 2021.
- [53] Ravi Garg, Vijay Kumar BG, Gustavo Carneiro, and Ian Reid. Unsupervised cnn for single view depth estimation: Geometry to the rescue. In *European Conference on Computer Vision*, pages 740–756. Springer, 2016.
- [54] Yue Luo, Jimmy Ren, Mude Lin, Jiahao Pang, Wenxiu Sun, Hongsheng Li, and Liang Lin. Single view stereo matching. In *Proceedings of the IEEE Conference on Computer Vision and Pattern Recognition*, pages 155–163, 2018.
- [55] Juan Luis GonzalezBello and Munchurl Kim. Forget about the lidar: Self-supervised depth estimators with med probability volumes. *Advances in Neural Information Processing Systems*, 33, 2020.
- [56] Reza Mahjourian, Martin Wicke, and Anelia Angelova. Unsupervised learning of depth and ego-motion from monocular video using 3d geometric constraints. In *Proceedings of the IEEE Conference on Computer Vision and Pattern Recognition*, pages 5667–5675, 2018.
- [57] Vincent Casser, Soeren Pirk, Reza Mahjourian, and Anelia Angelova. Depth prediction without the sensors: Leveraging structure for unsupervised learning from monocular videos. In *Proceedings of the AAAI Conference on Artificial Intelligence*, volume 33, pages 8001–8008, 2019.

- [58] Zhichao Yin and Jianping Shi. Geonet: Unsupervised learning of dense depth, optical flow and camera pose. In *Proceedings of the IEEE conference on computer vision and pattern recognition*, pages 1983–1992, 2018.
- [59] Yuliang Zou, Zelun Luo, and Jia-Bin Huang. Df-net: Unsupervised joint learning of depth and flow using cross-task consistency. In *Proceedings of the European conference on computer vision (ECCV)*, pages 36–53, 2018.
- [60] Yuhua Chen, Wen Li, Xiaoran Chen, and Luc Van Gool. Learning semantic segmentation from synthetic data: A geometrically guided input-output adaptation approach. In *Proceedings of the IEEE Conference on Computer Vision and Pattern Recognition*, pages 1841–1850, 2019.
- [61] Behzad Bozorgtabar, Mohammad Saeed Rad, Dwarikanath Mahapatra, and Jean-Philippe Thiran. Syndemo: Synergistic deep feature alignment for joint learning of depth and ego-motion. In *Proceedings of the IEEE International Conference on Computer Vision*, pages 4210–4219, 2019.
- [62] Johannes L Schönberger, Enliang Zheng, Jan-Michael Frahm, and Marc Pollefeys. Pixelwise view selection for unstructured multi-view stereo. In *European Conference on Computer Vision*, pages 501–518. Springer, 2016.
- [63] Mans Larsson, Erik Stenborg, Lars Hammarstrand, Marc Pollefeys, Torsten Sattler, and Fredrik Kahl. A cross-season correspondence dataset for robust semantic segmentation. In *Proceedings of the IEEE Conference on Computer Vision and Pattern Recognition*, pages 9532–9542, 2019.
- [64] Johannes L Schonberger and Jan-Michael Frahm. Structure-from-motion revisited. In *Proceedings of the IEEE Conference on Computer Vision and Pattern Recognition*, pages 4104–4113, 2016.
- [65] David G Lowe. Distinctive image features from scale-invariant keypoints. *International journal of computer vision*, 60(2):91–110, 2004.
- [66] Kaiming He, Georgia Gkioxari, Piotr Dollár, and Ross Girshick. Mask r-cnn. In *Proceedings of the IEEE international conference on computer vision*, pages 2961–2969, 2017.
- [67] Jianbo Jiao, Ying Cao, Yibing Song, and Rynson Lau. Look deeper into depth: Monocular depth estimation with semantic booster and attention-driven loss. In *Proceedings of the European conference on computer vision (ECCV)*, pages 53–69, 2018.
- [68] Jun-Yan Zhu, Taesung Park, Phillip Isola, and Alexei A Efros. Unpaired image-to-image translation using cycle-consistent adversarial networks. In *Proceedings of the IEEE international conference on computer vision*, pages 2223–2232, 2017.
- [69] Jian Xu, Chunheng Wang, Chengzuo Qi, Cunzhao Shi, and Baihua Xiao. Unsupervised semantic-based aggregation of deep convolutional features. *IEEE Transactions on Image Processing*, 28(2):601–611, 2018.
- [70] Assia Benbihi, Matthieu Geist, and Cédric Pradalier. Image-based place recognition on bucolic environment across seasons from semantic edge description. 2020.
- [71] Nathan Piasco, Désiré Sidibé, Valérie Gouet-Brunet, and Cedric Demonceaux. Learning scene geometry for visual localization in challenging conditions. In *2019 International Conference on Robotics and Automation (ICRA)*, pages 9094–9100. IEEE, 2019.
- [72] Nathan Piasco, Désiré Sidibé, Valérie Gouet-Brunet, and Cédric Demonceaux. Improving image description with auxiliary modality for visual localization in challenging conditions. *International Journal of Computer Vision*, pages 1–18, 2020.
- [73] Hyo Jin Kim, Enrique Dunn, and Jan-Michael Frahm. Learned contextual feature reweighting for image geolocalization. In *2017 IEEE Conference on Computer Vision and Pattern Recognition (CVPR)*, pages 3251–3260. IEEE, 2017.
- [74] Zhe Xin, Yinghao Cai, Tao Lu, Xiaoxia Xing, Shaojun Cai, Jixiang Zhang, Yiping Yang, and Yanqing Wang. Localizing discriminative visual landmarks for place recognition. In *2019 IEEE International Conference on Robotics and Automation (ICRA)*, 2019.
- [75] Huabing Zhou, Jiayi Ma, Chiu C Tan, Yanduo Zhang, and Haibin Ling. Cross-weather image alignment via latent generative model with intensity consistency. *IEEE Transactions on Image Processing*, 29:5216–5228, 2020.
- [76] Li Tang, Yue Wang, Qianhui Luo, Xiaqing Ding, and Rong Xiong. Adversarial feature disentanglement for place recognition across changing appearance. In *2020 IEEE International Conference on Robotics and Automation (ICRA)*, pages 1301–1307. IEEE, 2020.
- [77] Ziqiang Zheng, Yang Wu, Xinran Han, and Jianbo Shi. Forkgan: Seeing into the rainy night. In *The IEEE European Conference on Computer Vision (ECCV)*, August 2020.